
Article:
Morales, JE, Kim, J and Richardson, RR (2019) Geomagnetic Field Tracker for Deorbiting a CubeSat Using Electric Thrusters. Journal of Guidance, Control, and Dynamics, 42 (5). pp. 1157-1165. ISSN: 0731-5090

https://doi.org/10.2514/1.G003908

Geomagnetic Field Tracker for Deorbiting a CubeSat using Electric Thrusters

Jose E. Morales [*], Jongrae Kim[†], and Robert R. Richardson[‡]
Institute of Design, Robotics & Optimisation (iDRO)
School of Mechanical Engineering, University of Leeds
Leeds, LS2 9JT, the United Kingdom

I.Introduction

CUBESATS have gained popularity due to their small size, low cost and relative simplicity. CubeSats are deployed as 10 cm cubic blocks of up to 1.33 kg each, which can be combined in order to assemble systems of multiple units (1U, 2U, 3U and beyond). They provide easier access to space than traditional spacecraft, as they are considerable cheaper and their development time is also much shorter. Current and proposed applications include Earth observation [1], telecommunications [2], astronomy [3] and technology demonstrations in general. One of the main concerns, however, is their potential negative impact on the space debris problem.

It is estimated that a total of 24,000 objects that are 10 cm wide or larger were in orbit around the Earth as of 2011 [4]. Major collisions in space have already occurred, for instance, in 2009, American communications satellite Iridium 33 and the retired Russian Kosmos-2251 crashed, resulting in the destruction of both spacecraft and the generation of a large amount of orbital debris [5]. The Kessler syndrome [6] predicts that a critical density of objects in Low Earth Orbit (LEO) could be reached and that collisions between them could cause a cascade of impacts, that would eventually render some orbital ranges unusable within this century. Taking this into account, as well as the expected increase in CubeSat launch rates, it is critical that technologies are developed in order to deorbit these devices at the end of their operational life, thus preventing their accumulation in space. In a response to this, international guidelines require spacecraft to be deorbited or moved to a disposal orbit within 25 years of the end of their mission.

Several CubeSat deorbiting systems have been proposed over the past years, some of the most popular being the following: solar sails [7], inflatables [8], and electric tethers [9]. Sails rely on aerodynamic drag augmentation. NASA has been working in deorbiting sails technology, with their NanoSail-D and NanoSail-D2 [10] experiments. NanoSail-D was lost shortly after launch because of an anomaly in the launch vehicle, while its ground spare,

[1] PhD Researcher, School of Mechanical Engineering.
[†] Associate Professor, School of Mechanical Engineering.
[‡] Professor, School of Mechanical Engineering.

NanoSail-D2, was successfully launched to space in November 2010. After being deployed into a circular orbit of 650 km, the spacecraft deployed its sail, finally re-entering Earth's atmosphere on November 29, 2011, after spending 240 days in space, becoming the first successful demonstration of a deorbiting sail. The University of Surrey DeorbitSail satellite was successfully launched into orbit in 2015, however, the deployment of the sail was unsuccessful [11]. Finally, the University of Glasgow together with the company AAC Clyde Space have been working towards the development of the Aerodynamic End of Life Deorbit System for CubeSats (AEOLDOS) [7]. The system is currently commercially available, however, no references to deployment in space have been found to date.

Inflatable structures also rely on aerodynamic drag augmentation. Maessen et al. explore different shapes and determine a pyramidal structure to be optimal in their approach [8]. Similarly, Nakasuka et al. investigate the effectiveness of a spherical structure, proposing a system that would be effective for satellites at an initial orbit of up to 800 km [12]. Locku and Ash explore the design of inflatable structures with spherical, pyramidal and pillow shapes [13]. They claim that with this system, orbital decay times of 30 years can be attained for CubeSats in an initial 900 km orbit. Andrews et al. explore the concept of a cone shaped inflatable structure, which would not only allow the deorbiting of a CubeSat but also its survival during atmospheric re-entry phase, and would make possible the retrieval of payloads from CubeSats [14]. And, Viquerat et al. propose a combination between inflatable structures and sails, for its InflateSail CubeSat concept [15].

Finally, tethers interact with either the geomagnetic field or the plasma environment to generate drag forces. Voronka et al. propose the deployment of a 1 km long tether, in order to study the feasibility of their application to the deorbit of CubeSats [16]. Their simulations suggest that CubeSats at an initial orbit of 1000 km could be deorbited within 25 years. Zhu and Zhong have devoted much work to the application of space tethers to the deorbit of small spacecraft problem. With their analysis of the dynamics of an electrodynamic tether, they first explore the practicality of the technology [23–25]. Later, they propose an optimal On-Off control approach, where simulations show that the satellite system could lose 100 km of altitude within 60 days [20]. They develop a control system using a finite receding horizon control in order to achieve the optimal trajectory, which potentially would bring a tethered system from 800 km to 700 km within 25 days [21]. Janhunen [22] and Khurshid et al. [23] focus on the tether interaction with space plasma rather than the Earth's magnetic field. Their approach is applied in the Aalto-1 CubeSat as a technology demonstration mission [23].

A major disadvantage of these three approaches is that all of them require the deployment of actuators in space, which is technically challenging and make the system prone to failures. Further complications can come from the folding of sails and inflatables, which in turn require a considerable amount of volume. Recently, a new approach has emerged, which uses electric engines. Descriptions and working principles of five different types of electric engines can be found in [24–28]. These electric engines have low mass and volume, high specific impulse, do not require the deployment of actuators, and contain no movable parts, except for Micro Cathode Arc Thrusters and Micro Pulsed Plasma Thrusters, which contain springs, these being major advantages over the approaches already discussed. The idea of electric thrusters has been explored since 1960's. The first in space demonstration of electric propulsion was executed by the Space Electric Rocket Test (SERT-1) mission in 1964 [29]. Initially too bulky for its application in nanosatellites, this technology has evolved, and now electric engines are available in sizes and within budgets that make their integration in this class of satellites possible.

The application of electric thrusters to the CubeSat deorbit problem requires, however, to keep the thruster in the right direction to dissipate the kinetic energy of the CubeSat. A geomagnetic field tracker algorithm to be presented in this paper provides an effective and simple solution to control the orientation of CubeSat for deorbiting purposes. The algorithm only requires magnetometers, a GPS (Global Positioning Systems) receiver and magnetorquers, which are standard components in most of CubeSats. Because of the minimal requirements, together with its simplicity to implement the algorithm, it is an ideal algorithm for use within the stringent constraints present in nanosatellites.

This paper is organized as follows: Section II gives a summary of magnetorquers and electric propulsion. Section III describes the proposed deorbiting algorithm, as well as the respective stability and robustness analysis. Deorbiting phase simulations are presented in Section IV, and the conclusions are given in Section V.

II. Environment & Hardware

CubeSats are subject to volume, mass, and budget constraints and it is not always possible to equip them with the desired sensors and actuators. For example, traditional attitude determination algorithms, such as TRIAD and QUEST (Quaternion Estimation) require a minimum of two independent vector measurements [30]. These vectors are commonly obtained by a combination of magnetometers, Earth sensors, Sun sensors or star sensors. This requirement for multiple attitude sensors might be prohibitive for CubeSats. CubeSats usually also lack means for

propulsion, i.e., orbit housekeeping and orbital maneuvers in general are not possible. These restrictions have made the development of an effective deorbiting system for this class of satellites a rather challenging task.

A. Coordinates Systems & Geomagnetic Field

Three different coordinate systems are used in this work, which are the Earth Centered Inertial (ECI) frame, the Local Vertical Local Horizon (LVLH) frame, and the Body (B) frame. The ECI frame has its origin at the center of the Earth, the positive *x* axis points towards the point of vernal equinox, the positive *z* axis is aligned with the Earth rotation axis, and the positive *y* axis completes the right-handed frame. The LVLH frame has its origin at the center of mass of the CubeSat, the positive *z* axis points along the negative position vector, the positive *y* axis points along the negative orbit normal, and the positive *x* is defined by the cross product of *y* and *z* vectors. And, the B-frame has its origin at the center of mass of the satellite, and its axes in this paper are assumed to be aligned with the principal axes of the satellite.

Earth has a stable and steady magnetic field, whose variations are negligible compared to the usual time length of satellite mission. The International Geomagnetic Reference Field (IGRF-12) model provided by the International Association of Geomagnetism and Aeronomy (IAGA) is used in the numerical simulations presented later [31].

B. Magnetorquers and Magnetometers

Magnetorquers are the most common attitude actuators for CubeSats. Magnetorquers are light and small, do not have movable parts and do not need fuel. These features make them ideal for integration in nanosatellites. Magnetorquers generate a magnetic dipole, which interacts with Earth's magnetic field. The torque generated by this interaction is given by

$$\boldsymbol{\tau}_m = \mathbf{m} \times \mathbf{b} \tag{1}$$

where $\boldsymbol{\tau}_m$ is the torque in N·m, $\mathbf{m}$ is the 3x1 magnetic dipole vector produced by the magnetic torquers in $A \cdot m^2$, and $\mathbf{b}$ represents the 3x1 Earth's magnetic field vector in Tesla. Magnetorquers work in conjunction with magnetometers, which are the common attitude sensors in CubeSat because of its small size and light weight, and which are in charge of measuring the geomagnetic field, $\mathbf{b}$, in the B-frame.

C. Electric Propulsion

In terms of propulsion, several types of electrical engines are being developed for their integration in nanosatellites. A list of these engines includes; Electrospray [24], Pulsed Plasma Thrusters [25], Hall Effect Thruster [26], CubeSat Ambipolar Thruster [27], and Micro-Cathode Arc Thruster [28]. Table 1 summarizes some of the main features for each particular type of electric engine, with the aim to provide an insight of the potential that this technology has for applications in the field of CubeSats.

Table 1 Electric Propulsion Engines

Engine	Thrust, mN	Power, W	Fuel	Mass, g	Specific Impulse, s
Electrospray[§]	1.8	25	Ionic Salt	1400	1500
Micro Pulsed Plasma Thruster[**]	0.04	2	Teflon	280	600
Hall Effect Thruster[††]	0.1	3	Xenon	1000	1500
CubeSat Ambipolar Thruster [27]	0.5	50	Xenon	<1000	400
Micro Cathode Arc Thruster [32]	0.05	0.1	Solid fuel	200	2000

Note that the mass of these engines is still somewhat prohibitive for their use in 1U CubeSats except some unusual missions, as little or no room would be left for the rest of the systems and payload. However, their integration in the popular 3U or larger configuration seems feasible.

These electric propulsion technologies open the possibility for nanosatellite orbital control, including the crucial phase of deorbiting. In the following section, an algorithm that enables the use of electrical engines for CubeSat with this objective is presented.

D. Attitude Kinematics & Attitude Dynamics

Satellite attitude kinematics are given as

$$\dot{\mathbf{q}} = \frac{1}{2}\begin{bmatrix} -[\boldsymbol{\omega}\times] & \boldsymbol{\omega} \\ -\boldsymbol{\omega}^{T} & 0 \end{bmatrix}\mathbf{q} \tag{2}$$

where $\mathbf{q}$ is the 4x1 quaternion representing the relative attitude of the B-frame with respect to the ECI frame, $\dot{\mathbf{q}}$ is the time derivative of the quaternion, $\boldsymbol{\omega}$ is the 3x1 angular velocity vector of the body frame with respect to the

[§] Data available online at https://static1.squarespace.com/static/5446faa2e4b025843cfc6731/t/58b0893120099e71f22ca0c8 [retrieved 23 April 2018].
[**] Data available online at https://mars-space.co.uk/ppt [retrieved 23 April 2018].
[††] Data available online at http://www.unisec-global.org/ddc/pdf/1st/09_PaulLascombes_abst.pdf [retrieved 25 April 2018].

inertial frame expressed in the body frame, and $[\boldsymbol{\omega}\times]$ is the 3x3 matrix defined such that $[\mathbf{a}\times]\mathbf{b} = \mathbf{a}\times\mathbf{b}$, $\mathbf{a}$ and $\mathbf{b}$ are 3x1 vectors. Attitude dynamics of the satellite are expressed through the Euler's rotation equation as follows:

$$\dot{\boldsymbol{\omega}} = \mathbf{J}^{-1}\left(-\boldsymbol{\omega}\times\mathbf{J}\boldsymbol{\omega} + \boldsymbol{\tau}_{\text{tot}}\right) = \mathbf{g}\left(\boldsymbol{\omega}, \boldsymbol{\tau}_{\text{tot}}\right) \tag{3}$$

where $\mathbf{J}$ is the 3x3 inertia tensor of the satellite, and $\boldsymbol{\tau}_{\text{tot}}$ is the 3x1 vector representing the sum of all external torques, which include control torques as well as perturbation torques caused by the environment such as solar radiation pressure, gravity gradient, and atmospheric drag.

III. Geomagnetic Field Tracker & Stability Analysis

In this section, the geomagnetic field tracker is presented for deorbiting a CubeSat. The closed-loop system with the geomagnetic field tracker is derived, which is given by a linear periodically time-varying system. The stability analysis is performed for the time-varying system using the Floquet theorem.

A. Control Law

To deorbit satellites using a thruster, it first needs to be oriented in a desired direction which ensures that the thrust vector opposes the direction of the orbital velocity. The control algorithm aligns the satellite attitude to the geomagnetic field vector using magnetorquers so that the thruster can dissipate the kinetic energy of the nanosatellite during half of the orbit. Only one attitude sensor, magnetometer, is required, which is relatively small, compact and cheap, and integrated in many CubeSats missions. This will provide the magnetic field vector reading in the B-frame. A GPS receiver, is needed to determine when the thruster must be fired to deorbit the satellite. The orbital position and velocity in the ECI frame are provided by the GPS receiver.

The objective of the attitude control algorithm is to align the $+x$ body axis with the local magnetic vector. In order to accomplish this, the desired torque is given by

$$\boldsymbol{\tau}_{\text{des}} = k_1\mathbf{e} \tag{4}$$

where k_1 is a control gain to be designed,

$$\mathbf{e} = \mathbf{i}\times\hat{\mathbf{b}} \tag{5}$$

i is the unit vector towards the +*x* direction of the B-frame, and $\hat{\mathbf{b}}$ is the normalized magnetic field in the B-frame, which is equal to **b**/||**b**||, where ||**b**|| is the magnitude of **b**. The commanded magnetic dipole for the magnetorquers to generate the desired torque can be obtained using Eq. (1). Including additional damping effect, the geomagnetic field tracker dipole becomes

$$\mathbf{m}_{\text{ctrl}} = k_1 \left[\hat{\mathbf{b}} \times \right] \mathbf{e} - k_2 \frac{d^{\text{B}}}{dt} \hat{\mathbf{b}} \tag{6}$$

where k_2 is another control gain to be designed and d^{B} / dt is the time derivative in the B-frame, which could be implemented using the finite-difference approximation the same way that the B-dot controller is implemented [33]. Note that a similar control algorithm was proposed by Jan and Tsai for initial attitude acquisition [34]. Eq. (6) can be directly implemented with a numerical differentiator to approximate the time derivative of geomagnetic field vector measurement. If a rate gyro sensor is available, then $d^{\text{B}}\left(\hat{\mathbf{b}}\right) / dt$ can be replaced by $\left[\hat{\mathbf{b}} \times \right] \boldsymbol{\omega}$. Hence,

$$\mathbf{m}_{\text{ctrl}} = k_1 \left[\hat{\mathbf{b}} \times \right] \mathbf{e} - k_2 \left[\hat{\mathbf{b}} \times \right] \boldsymbol{\omega} \tag{7}$$

Figure 1 shows the CubeSat alignment with the geomagnetic field vector, as well as the relative attitude to the spacecraft velocity vector, which determines when the thrusters (mounted in the +*x* face of the satellite) can be fired and when they should be turned off. An interesting instance is observed in Fig. 1 when the satellite is above the north pole. Intuitively, it might seem that having the thruster activated over the north pole would push the satellite upwards, i.e., gaining the altitude. However, the objective of the deorbiting algorithm is to dissipate the kinetic energy of the satellite and it leads to lower the altitude. This is achieved whenever the thrust vector has a component that opposes the velocity vector.

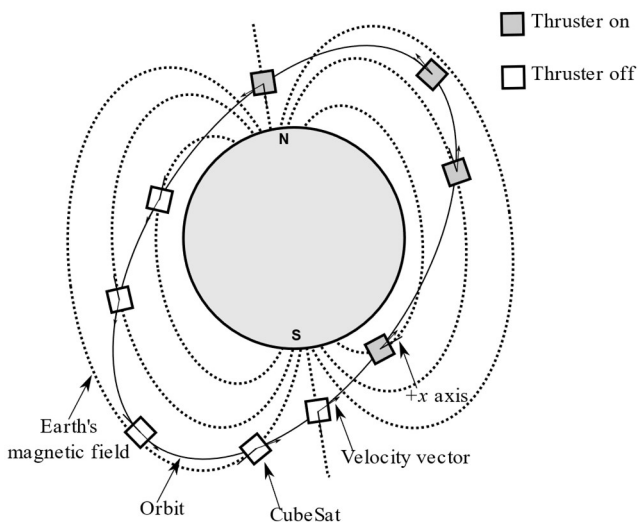

Fig. 1 CubeSat +*x* axis aligned with magnetic field and relative attitude respect to velocity vector.

Once the CubeSat's +*x* face is tracking the magnetic field vector, it can be determined when to activate the thrusters, in order to cause the loss of orbital energy. This knowledge comes from the fact that the magnetic field vector is available in LVLH frame, $\mathbf{b}^{lvlh} = \begin{bmatrix} b_x^{lvlh} & b_y^{lvlh} & b_z^{lvlh} \end{bmatrix}^T$, where $(\bullet)^T$ is the transpose. Because of the relationship between the orbital velocity vector ***v*** and the +*x* axis in the LVLH frame, the thrust vector opposes the direction of travel at some degree when the component b_x^{lvlh} is positive, which implies the thruster points in the direction of travel as shown in Fig. 2. In Fig. 2, it is important to clarify that the +*x* axis of the LVLH frame does not necessarily coincide with the velocity vector, however, in a quasi-circular orbit this is a reasonable simplification.

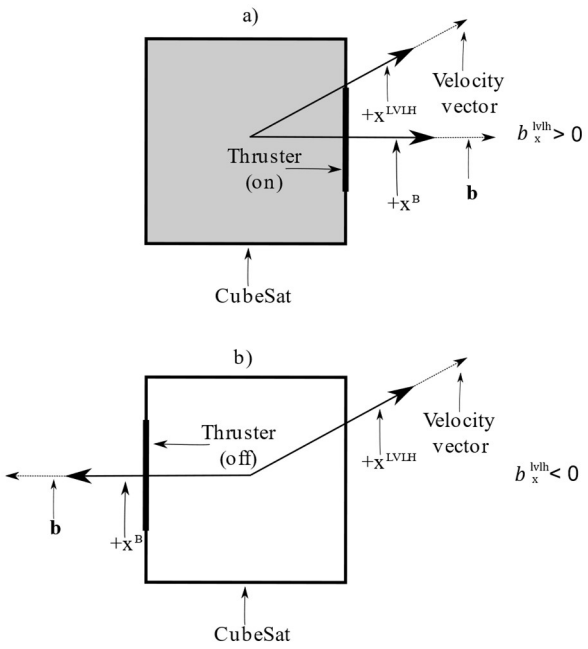

Fig. 2 CubeSat attitude cases to deorbit: a) attitude where the thruster is on or b) off.

Nonlinear simulations were performed to evaluate the tracking error of the algorithm, which is the angle difference between the magnetic field vector and the $+x$ body axis of the satellite. In all the following simulations within this paper, we consider a 3U CubeSat, equipped with three orthogonal magnetorquers, a three axes magnetometer, a three axes rate gyro, a GPS receiver, which is one of the standard CubeSat configurations, and an electric engine for propulsion, whose thruster vector direction is assumed to be aligned with the $+x$ face of the satellite. The CubeSat has a mass of 3.5 kg and the diagonal terms of the inertia tensor are [0.01; 0.0506; 0.0506] kg·m^2. It has an initial orbital altitude of 900 km, in a near circular orbit. The inclination is set to 65 degrees. The control gains are tuned such that $k_1 = 0.5$ and $k_2 = 25$ through multiple trial and error procedures. Initially, the gains are varied to identify a coarse range of the feasible gains and a fine tuning is performed to determine the final gains in aligning the body axis to the magnetic field vector. It is also important to mention that in practice, magnetometers and magnetorquers cannot be activated at the same time, as the magnetometers measurements would be affected by the magnetorquers. Therefore, a duty cycle is implemented, where during a period of 5 seconds, magnetorquers are active for the first 4s and magnetometers are active for the remaining 1s. All simulations were performed using Matlab/Simulink with the default numerical integration algorithm and the relative tolerance of 0.001.

Figure 3 shows the evolution of tracking angle error through the whole deorbiting process with electrospray thruster. It can be seen that after an initial error of about 100 degrees, the CubeSat is able to track the magnetic vector within an accuracy of roughly 5 degrees. High pointing accuracy is not required for the deorbit phase of the mission, therefore, this performance is acceptable.

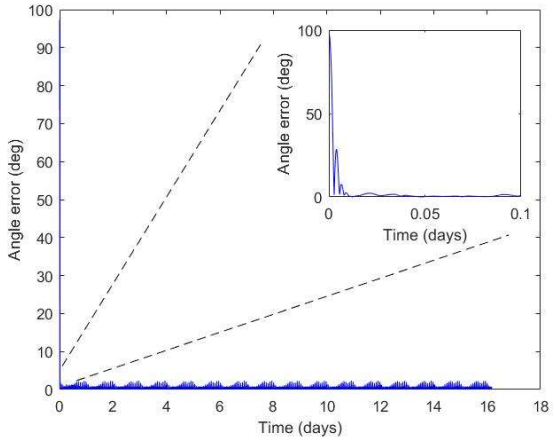

Fig. 3 Magnetic vector tracking error.

B. Stability Analysis

To provide a stability analysis of the geomagnetic field tracking mode of CubeSat, a linearization is performed. Firstly, taking the time derivative of Eq. (5) as follows:

$$\dot{\mathbf{e}} = \left(\boldsymbol{\omega} \times \mathbf{i}\right) \times \hat{\mathbf{b}} = -\left[\hat{\mathbf{b}} \times\right]\left[\boldsymbol{\omega} \times\right]\mathbf{i} = \mathbf{f}\left(\hat{\mathbf{b}}, \boldsymbol{\omega}\right) \tag{8}$$

Note that the desired equilibrium state is $\mathbf{e} = \begin{bmatrix} 0 & 0 & 0 \end{bmatrix}^T$ and $\boldsymbol{\omega} = \begin{bmatrix} \omega_x & 0 & 0 \end{bmatrix}^T$, where ω_x is a rotation rate allowed in the $+x$ axis of the satellite, which is not required to be zero. The equilibrium point also implies that the nominal normalized magnetic field vector in the B-frame is given by $\hat{\mathbf{b}} = \begin{bmatrix} 1 & 0 & 0 \end{bmatrix}$. The linearized system is expressed as follows:

$$\dot{\mathbf{x}} = \begin{bmatrix} \dfrac{\partial \mathbf{f}\left(\hat{\mathbf{b}},\boldsymbol{\omega}\right)}{\partial \mathbf{e}} & \dfrac{\partial \mathbf{f}\left(\hat{\mathbf{b}},\boldsymbol{\omega}\right)}{\partial \boldsymbol{\omega}} \\ \dfrac{\partial \mathbf{g}\left(\boldsymbol{\omega},\boldsymbol{\tau}_{\text{tot}}\right)}{\partial \mathbf{e}} & \dfrac{\partial \mathbf{g}\left(\boldsymbol{\omega},\boldsymbol{\tau}_{\text{tot}}\right)}{\partial \boldsymbol{\omega}} \end{bmatrix} \mathbf{x} + \begin{bmatrix} \dfrac{\partial \mathbf{f}\left(\hat{\mathbf{b}},\boldsymbol{\omega}\right)}{\partial \mathbf{m}_{\text{ctrl}}} \\ \dfrac{\partial \mathbf{g}\left(\boldsymbol{\omega},\boldsymbol{\tau}_{\text{tot}}\right)}{\partial \mathbf{m}_{\text{ctrl}}} \end{bmatrix} \mathbf{m}_{\text{ctrl}} \tag{9}$$

Once the Jacobian equations are solved, a 6x6 state matrix is obtained, and it is noticed that the first and the fourth rows and columns are all zero. This is due to the fact that the control torque, Eq. (4), is always perpendicular to the +*x* axis of the satellite at the equilibrium point. Therefore, it has no components in the +*x* axis of the B-frame and the rotational motion about this axis is allowed in the geomagnetic field tracking mode. Hence, a reduced dimension linearized system is given by

$$\dot{\mathbf{x}}_r = \mathbf{A}_r \mathbf{x}_r + \mathbf{B}_r\left(t\right)\mathbf{K}_r \mathbf{x}_r \tag{10}$$

where $\mathbf{K}_r\mathbf{x}_r$ is a compact form of Eq. (7)

$$\mathbf{A}_r = \begin{bmatrix} 0 & -\omega_x & -1 & 0 \\ \omega_x & 0 & 0 & -1 \\ 0 & 0 & 0 & \sigma_2\omega_x \\ 0 & 0 & \sigma_3\omega_x & 0 \end{bmatrix}, \tag{11}$$

$$\mathbf{B}_r\left(t\right) = \begin{bmatrix} 0 & 0 & 0 & \dfrac{-b_x}{J_{zz}} \\ 0 & 0 & \dfrac{b_x}{J_{yy}} & 0 \end{bmatrix}^T, \tag{12}$$

$$\mathbf{K}_r = \begin{bmatrix} 0 & -k_1 & 0 & k_2 \\ k_1 & 0 & -k_2 & 0 \end{bmatrix}, \tag{13}$$

$$\mathbf{x}_r = \begin{bmatrix} e_y & e_z & \omega_y & \omega_z \end{bmatrix}^T, \tag{14}$$

ω_x is assumed to be a constant, $\sigma_2 = (-J_{xx} + J_{zz})/J_{yy}$, and $\sigma_3 = (J_{xx}\text{-}J_{yy})/J_{zz}$.

The resultant closed loop system can then be expressed as follows:

$$\dot{\mathbf{x}}_r = \mathbf{A}_{\text{CL}}\left(t\right)\mathbf{x}_r \tag{15}$$

where

$$\mathbf{A}_{\mathrm{CL}}(t) := \mathbf{A}_r + \mathbf{B}_r(t)\mathbf{K}_r \tag{16}$$

As the geomagnetic field is periodic along the orbit, the time varying matrix $\mathbf{A}_{\mathrm{CL}}(t)$ is also periodic as follows:

$$\mathbf{A}_{\mathrm{CL}}(t) = \mathbf{A}_{\mathrm{CL}}(t+T) \tag{17}$$

where T is the period of the system equal to the orbit period. Since the system is now expressed in linear periodic time varying form, Floquet theory can be used for the stability analysis. A brief summary of Floquet theory is provided next and more details can be found in [34].

Define a constant matrix **F** such that

$$e^{\mathbf{F}\mathrm{T}} = \mathbf{\Phi}(T,0) \tag{18}$$

where the following equations must be satisfied:

$$\mathbf{\Phi}(t,\tau) = \mathbf{L}(t)e^{(t-\tau)\mathbf{F}}\mathbf{L}^{-1}(\tau) \tag{19}$$

$$\mathbf{L}(t+T) = \mathbf{L}(t) \tag{20}$$

$\mathbf{\Phi}(\cdot,\cdot)$ is the state transition matrix, $\mathbf{L}(t)$ is the solution of the following two point boundary value problem [35]:

$$\dot{\mathbf{L}}(t) = \mathbf{A}_{\mathrm{CL}}(t)\mathbf{L}(t) - \mathbf{L}(t)\mathbf{F} \tag{21a}$$

$$\dot{\mathbf{F}}(t) = 0 \tag{21b}$$

the boundary conditions are given by $\mathbf{L}(t_0) = \mathbf{I}_4$ and $\mathbf{L}(t_0+2T) = \mathbf{I}_4$, and $\mathbf{I}_4$ is the 4x4 identity matrix. The linear periodic time-varying system given by Eq. (15) is exponentially stable if and only if **F** is Hurwitz, i.e., all real parts of the eigenvalues are negative.

Floquet analysis was performed for a range of ω_x values that goes from -10 deg/s to 10 deg/s. Figure 4 shows the maximum real part of eigenvalues of **F**, which are always negative. Hence, the stability of the geomagnetic field tracking system for the given range of ω_x is verified.

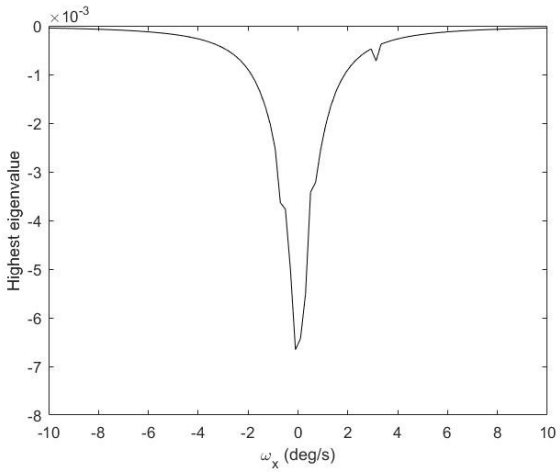

Fig. 4 Floquet stability analysis results.

IV. Deorbiting Performance & Robustness Analysis

A deorbit scenario was simulated in order to test the performance of the proposed algorithm. Aerodynamic drag accelerations are taken into account for this numerical analysis, using the U.S. Standard Atmosphere 1976 model. Gaussian perturbation equations were used in order to compute the evolution of the orbital parameters [36]. The deorbit process is simulated for the five different types of electric engines shown in Table 1. The time span for each simulation scenario is 20 days, unless the deorbiting operation is achieved in less time.

A. Deorbiting

Figure 5 shows the evolution of the orbital altitudes for each of the five engines scenarios. The first effect that is apparent from these charts is that the eccentricity of the orbit is gradually increased. This comes from the fact that the thrust is applied during only one half of the orbit. It also can be seen from Fig. 5 a), that once the perigee of the orbit reaches denser layers of the atmosphere, the orbit quickly falls into a critical altitude of around 100 km, when the CubeSat can be considered to be deorbited.

The deorbit times are of course inversely proportional to the thrust that the engines can provide, with the better performance obtained with Electrospray engines, with a deorbit time of roughly 16 days, followed by the CubeSat Ambipolar thruster, that decreases the perigee of thee satellite by about 250 km in 20 days. An important aspect to take into account here, is the operational lifetime of each engine, which has the potential to determine if the engine can be active during the whole deorbit operation, or if it can be used to lower the perigee to an altitude where

aerodynamic drag can take over and deorbit the satellite within time span required by international guidelines. According to the references in Table 1, Electrospray engine has a lifetime of about 650 hours, which would be enough to carry the entire deorbit operation. In the case of Micro Pulsed Plasma thruster, state of the art technology only would allow to decrease the perigee of a 3U CubeSat by about 40 km, therefore, further advancements in this specific engine technology are necessary for their practical use in deorbit operations. Finally, for Hall Effect thrusters, it is claimed that they are expected to be able to deorbit a 3U CubeSat from an initial orbit of 750 km. Although no mention of an algorithm is made, this gives confidence that the application of this type of engine to the deorbit problem is practical. No information regarding the lifetime of CubeSat Ambipolar Thruster and Micro Cathode Arc Thruster was found.

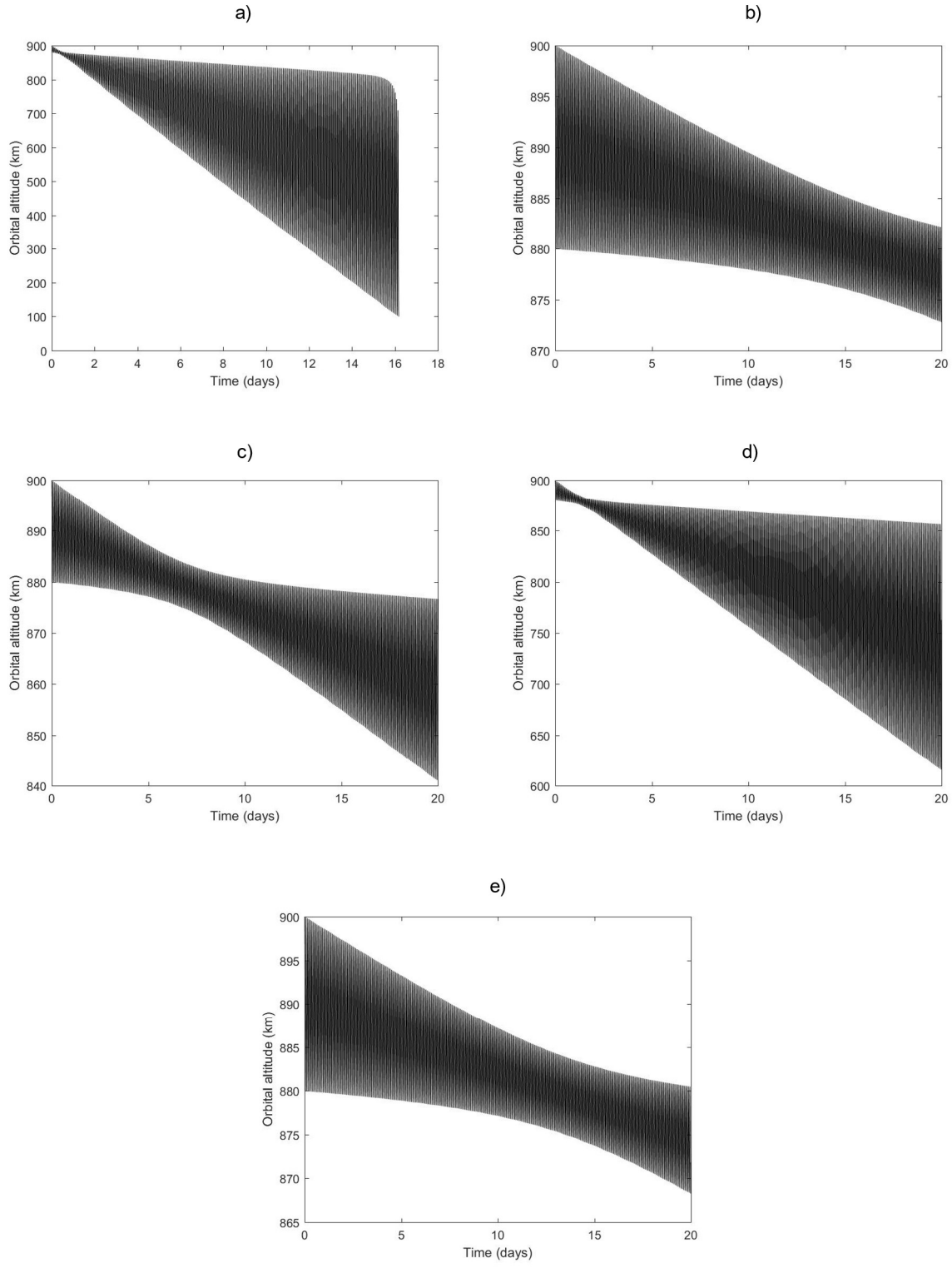

Fig. 5 Deorbiting rates a) Electrospray thruster; b) Micro Pulsed Plasma Thruster; c) Hall Effect thruster; d) CubeSat Ambipolar thruster; and e) Micro Cathode Arc thruster.

Another interesting aspect to look at is the evolution of the semi-major axis. Figure 6 depicts this metric for the electrospray scenario, where a step pattern can be observed. This is also an effect of the thrust being applied during only half of the orbit.

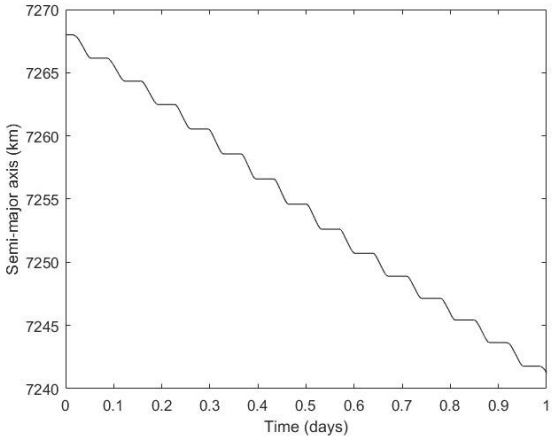

Fig. 6 Semi-major axis evolution using electrospray thruster.

The system state and control inputs for the Electrospray scenario case are shown Figs 7 - 10. Figure 7 shows the quaternion evolution. As shown in Fig. 8, the angular rates are kept at low including ω_x, an axis where little or no control torques can be applied. Figure 9 depicts the control magnetic dipoles, it can be seen that after an initial saturation in m_x and m_z, the control action is very small during the rest of the process, in the order of 0.02 $A \cdot m^2$. As expected, m_x control action is virtually zero once the satellite is tracking the magnetic vector. Finally, Fig. 10 shows the action of the thruster, where the thrusters are only active during half the orbital period.

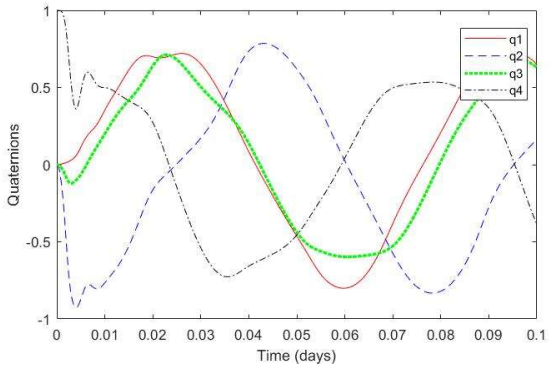

Fig. 7 CubeSat attitude in quaternions.

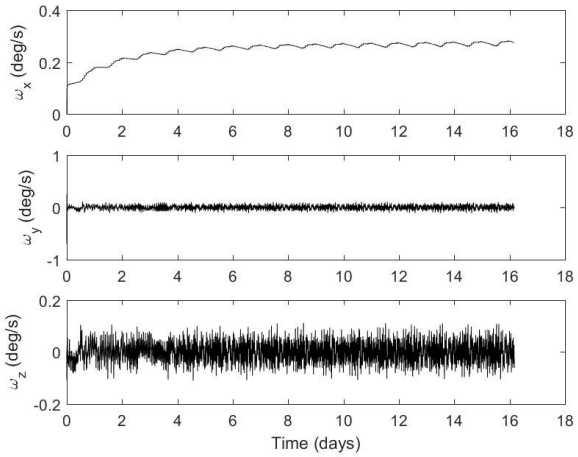

Fig. 8 CubeSat angular velocities.

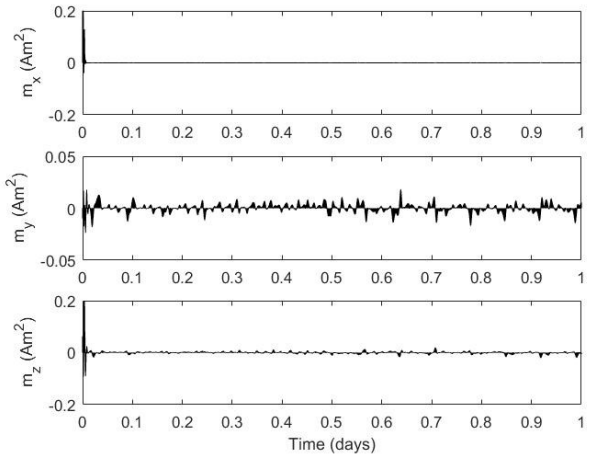

Fig. 9 Control magnetic dipoles.

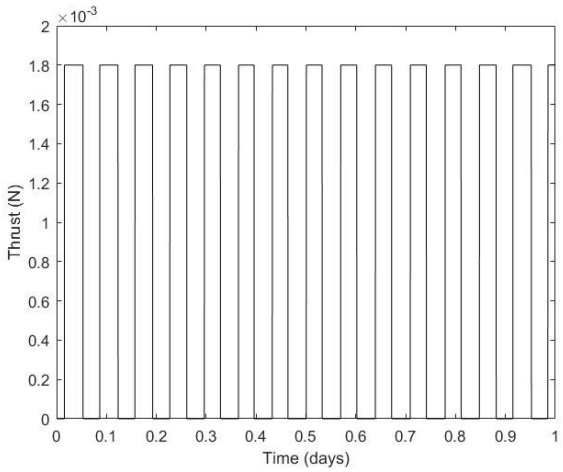

Fig. 10 Thruster activation.

B. Robustness Analysis

Full nonlinear robustness analysis of the deorbiting algorithm is performed through Monte Carlo simulations. An uncertainty vector Δ is defined considering uncertainties in the mass, the inertia tensor, as well as the initial conditions in terms of orbital parameters and initial attitude. Detailed explanation of the Δ vector components is given in Table 2. The work of Cortiella et al. was taking as a reference for the values of the non-diagonal elements of the inertia tensor [37]. The electrospray scenario was considered, and a total of 1000 runs were executed, with the results shown in Fig. 11.

Table 2 Uncertainties vector

Uncertainty	Parameter	Range	Formula
δm	Mass	±0.1	$\tilde{m} = m(1 + \delta m)$
δJ_{xx}	Inertia tensor x axis	[0, 0.03]	$\tilde{J}_{xx} = J_{xx} + \delta J_{xx}$
δJ_{yy}	Inertia tensor y axis	±0.1	$\tilde{J}_{yy} = J_{yy}(1 + \delta J_{yy})$
δJ_{zz}	Inertia tensor z axis	±0.1	$\tilde{J}_{zz} = J_{zz}(1 + \delta J_{zz})$
δJ_{ij}	Inertia tensor non-diagonal elements	[-0.001, 0]	$\tilde{I}_{ij} = \delta I_{ij}$
δa	Semi major axis	±0.1	$\tilde{a} = a + \delta a * 100000$
δe	Eccentricity	±0.1	$\tilde{e} = e(1 + \delta e)$

δi	Inclination	±0.1	$\tilde{\imath} = i(1 + \delta i)$
$\delta\omega_p$	Argument of perigee	±0.1	$\tilde{\omega}_p = \omega_p(1 + \delta\omega_p)$
$\delta\Omega$	Right ascension of the ascending node	±0.1	$\tilde{\Omega} = \Omega(1 + \delta\Omega)$
δM	Mean anomaly	±0.1	$\tilde{M} = M(1 + \delta M)$
$\boldsymbol{\delta q_0}$	Initial attitude quaternion		Uniform Random
$\boldsymbol{\delta\omega_0}$	Initial angular velocity vector	±0.017	$\tilde{\boldsymbol{\omega}}_{\mathbf{0}} = \delta\boldsymbol{\omega}_{\boldsymbol{o}}$

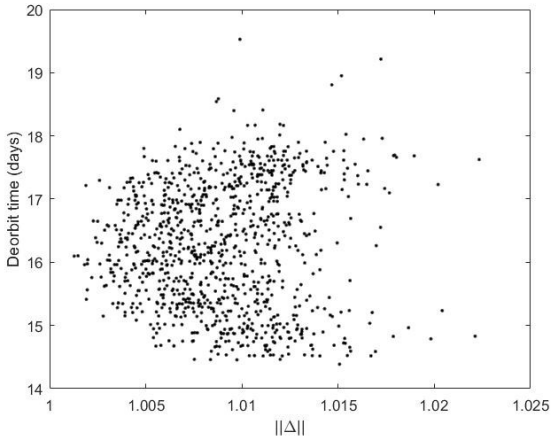

Fig. 11 Robustness analysis with Monte Carlo simulations.

It can be seen that even in the presence of uncertainties, the deorbiting algorithm performs well, and a maximum deorbit time of less than 20 days in the electrospray engine case can be achieved.

V.Conclusions

An efficient and simple attitude tracking algorithm for deorbiting a CubeSat is presented. Stability of the proposed tracking algorithm is proved through Floquet Analysis. With the tracking algorithm, de-orbiting performances for five different types of electric engines are demonstrated. Robustness of the de-orbiting algorithm in the presence of uncertainties is shown through the Monte Carlo simulations. Future works include showing the efficiency of the algorithm for various CubeSats configurations and developing optimal control gain procedures to

minimize the usage of control energy. The simplicity of the proposed algorithm and the minimal requirements for sensors and actuators are the most important advantages. It allows this algorithm to be suitable for implementation in many CubeSats with the existing specifications.

Acknowledgments

The authors would like to thank Consejo Nacional de Ciencia y Tecnología (CONACyT) in Mexico for their financial support during this work. The Monte-Carlo simulations were undertaken on ARC2, part of the High Performance Computing (HPC) facilities at the University of Leeds, Leeds, UK.

References

[1] A. Nascetti, E. Pittella, P. Teofilatto, and S. Pisa, "High-Gain S-band Patch Antenna System for Earth-Observation CubeSat Satellites," *IEEE Antennas Wirel. Propag. Lett.*, vol. 14, pp. 434–437, 2015.
doi: 10.1109/LAWP.2014.2366791.

[2] R. E. Hodges, D. J. Hoppe, M. J. Radway, and N. E. Chahat, "Novel deployable reflectarray antennas for CubeSat communications," *2015 IEEE MTT-S Int. Microw. Symp. IMS 2015*, pp. 4–7, 2015.
doi: 10.1109/MWSYM.2015.7167153.

[3] J.-P. Park *et al.*, "CubeSat Development for CANYVAL-X Mission," in *SpaceOps Conferences*, Daejeon, Korea, 2016.
doi: 10.2514/6.2016-2493.

[4] S. Chen, "The space Debris problem," *Asian Perspect.*, vol. 35, no. 4, pp. 537–558, 2011.

[5] D. L. Oltrogge and K. Leveque, "An Evaluation of CubeSat Orbital Decay," in *25th Annual AIAA/USU Conference on Small Satellites*, 2011.

[6] D. J. Kessler and B. G. Cour-Palais, "Collision frequency of artificial satellites: The creation of a debris belt," *J. Geophys. Res.*, 1978.
doi: 10.1029/JA083iA06p02637.

[7] P. Harkness, M. McRobb, P. Lützkendorf, R. Milligan, A. Feeney, and C. Clark, "Development status of AEOLDOS - A deorbit module for small satellites," *Adv. Sp. Res.*, 2014.
doi: 10.1016/j.asr.2014.03.022.

[8] D. Maessen, E. van Breukelen, B. T. C. Zandbergen, and O. K. Bergsma, "Development of a generic inflatable de-orbit device for CubeSats," in *Proceedings of the 58th International Astronnautical Congress*, Hyderabad, India, 2007.

[9] R. P. Hoyt, I. M. Barnes, N. R. Voronka, and J. T. Slostad, "The Terminator Tape™: A Cost-Effective De-Orbit module

for End-of-Life Disposal of LEO Satellites," in *AIAA Space 2009 Conference and Exposition*, Pasadena, California, 2009.
doi: 10.2514/6.2009-6733.

[10] L. Johnson, M. Whorton, A. Heaton, R. Pinson, G. Laue, and C. Adams, "NanoSail-D : A solar sail demonstration mission," *Acta Astronaut.*, vol. 68, pp. 571–575, 2011.
doi: 10.1016/j.actaastro.2010.02.008.

[11] O. R. O. Stohlman, M. Schenk, and V. Lappas, "Development of the Deorbitsail flight model," in *Spacecraft Structures Conference*, National Harbor, Maryland, USA, 2014.
doi: 10.2514/6.2014-1509.

[12] S. Nakasuka, K. Senda, A. Watanabe, T. Yajima, and H. Sahara, "Simple and Small De-orbiting Package for Nano-Satellites Using an Inflatable Balloon," in *Trans. JSASS Space Tech. Japan*, 2009.
doi: 10.2322/tstj.7.Tf_31.

[13] E. Lokcu and R. L. Ash, "A de-orbit system design for CubeSat payloads," in *RAST 2011 - Proceedings of 5th International Conference on Recent Advances in Space Technologies*, Istanbul, 2011.
doi: 10.1109/RAST.2011.5966879.

[14] J. Andrews, K. Watry, and K. Brown, "Nanosat Deorbit and Recovery System to Enable New Missions," *25th Annu. AIAA/USU Conf. Small Satell.*, 2011.

[15] A. Viquerat, M. Schenk, B. Sanders, and V. Lappas, "Inflatable Rigidisable Mast For End-Of-Life Deorbiting System," in *European Conference on Spacecraft Structures, Materials and Environmental Testing (SSMET)*, Braunschweig, Germany, 2014.

[16] N. R. Voronka *et al.*, "Technology Demonstrator of a Standardized Deorbit Module Designed for CubeSat and RocketPod Applications," in *19th Annual AIAA/USU Conference on Small Satellites*.

[17] Z. H. Zhu and R. Zhong, "Deorbiting Dynamics of Electrodynamic Tether," *Int. J. Aerosp. Light. Struct.* -, 2011.
doi: 10.3850/2010428611000043.

[18] R. Zhong and Z. H. Zhu, "Libration dynamics and stability of electrodynamic tethers in satellite deorbit," *Celest. Mech. Dyn. Astron.*, pp. 279–298, 2013.
doi: 10.1007/s10569-013-9489-4.

[19] R. Zhong and Z. H. Zhu, "Dynamics of nanosatellite deorbit by bare electrodynamic tether in low earth orbit," *J. Spacecr. Rockets*, pp. 691–700, 2013.
doi: 10.2514/1.A32336.

[20] R. Zhong and Z. H. Zhu, "Optimal Current Switching Control of Electrodynamic Tethers for Fast Deorbit," *J. Guid.*

Control. Dyn., pp. 1501–1511, 2014.
doi: 10.2514/1.G000385.

[21] R. Zhong and Z. H. Zhu, "Optimal Control of Nanosatellite Fast Deorbit Using Electrodynamic Tether," *J. Guid. Control. Dyn.*, pp. 1182–1194, 2014.
doi: 10.2514/1.62154.

[22] P. Janhunen, "Simulation study of the plasma-brake effect," *Ann. Geophys.*, pp. 1207–1216, 2014.
doi: 10.5194/angeo-32-1207-2014.

[23] O. Khurshid, T. Tikka, J. Praks, and M. Hallikainen, "Accommodating the plasma brake experiment on-board the Aalto-1 satellite," *Proc. Est. Acad. Sci.*, 2014.
doi: 10.3176/proc.2014.2S.07.

[24] A. H. Schouten and F. Martel, "Design and Characterization of a Scalable ion Electrospray Propulsion System," in *30th International Symposium on Space Technology and Science*, Hyogo-Kobe, Japan, 2015, pp. 1–11.

[25] M. Coletti, F. Guarducci, and S. B. Gabriel, "A micro PPT for Cubesat application : Design and preliminary experimental results," *Acta Astronaut.*, vol. 69, no. 3–4, pp. 200–208, 2011.
doi: 10.1016/j.actaastro.2011.03.008.

[26] J. W. Dankanich *et al.*, "The iodine Satellite (iSAT) Hall Thruster Demonstration Mission Concept and Development," pp. 1–13, 2013.

[27] T. A. Collard, F. H. Ebersohn, and B. W. Longmier, "Initial Operation of the CubeSat Ambipolar Thruster," in *30th International Symposium on Space Technology and Science*, Hyogo-Kobe, Japan, 2015, pp. 1–12.
doi: 10.1109/PLASMA.2015.7179981.

[28] T. Zhuang, A. Shashurin, D. Chiu, G. Teel, and A. E. Washington, "Micro-Cathode Arc Thruster Development and Characterization," in *International Electric Propulsion Conference*, Wiesbaden, Germany, 2011, vol. 1, pp. 1–7.

[29] R. J. Cybulski, D. M. Shellhammer, R. R. Lovell, E. J. Domino, and J. T. Kotnik, "Results From SERT I Ion Rocket Flight Test," 1965.

[30] M. D. Shuster and S. D. Oh, "Three-axis attitude determination from vector observations," *J. Guid. Control. Dyn.*, vol. 4, no. 1, pp. 70–77, 1981.
doi: 10.2514/3.19717.

[31] J. Davis and V. Tech, "Mathematical Modeling of Earth ' s Magnetic Field." Virginia Polytechnic Institute and State Univ, Blacksburg, VA, pp. 1–21, 2004.

[32] M. Keidar, "Micro - Cathode Arc Thruster for Small Satellite Propulsion," in *2016 IEEE Aerospace Conference*, Big Sky, Montana, 2016.

doi: 10.1109/AERO.2016.7500506.

[33] A. C. Stickler, and K. T. Alfriend, "An Elementary Magnetic Attitude Control System," *Mechanics and Control of Flight Conference,* Anaheim, California, 1974.
doi: 10.2514/6.1974-923.

[34] Y. W. Jan and J. R. Tsai, "Active control for initial attitude acquisition using magnetic torquers," *Acta Astronaut.*, vol. 57, no. 9, pp. 754–759, 2005.
doi: 10.1016/j.actaastro.2005.03.067.

[35] H. K. Khalil, *Nonlinear Systems*, 2nd ed. New Jersey: Prentice-Hall, 1996.

[36] J. Kim, D. G. Bates, and I. Postlethwaite, "Robustness analysis of linear periodic time-varying systems subject to structured uncertainty," *Syst. Control Lett.*, vol. 55, no. 9, pp. 719–725, 2006.
doi: 10.1016/j.sysconle.2006.02.005.

[37] D. A. Vallado, *Fundamentals of Astrodynamics and Applications*, 3rd ed. New York: Microcosm Press, 2007.

[38] A. Cortiella *et al.*, "3CAT-2: Attitude determination and control system for a GNSS-R earth observation 6U cubesat mission," *Eur. J. Remote Sens.*, vol. 49, no. June, pp. 759–776, 2016.
doi: 10.5721/EuJRS20164940.